Catalytic conversion of glycerol to bio-based aromatics using H-ZSM-5 in combination with various binders

He, Songbo; Goldhoorn, Hero Reinder; Tegudeer, Zhuorigebatu; Chandel, Anshu; Heeres, Andre; Liu, Chuncheng; Pidko, Evgeny; Heeres, Hero Jan

DOI
10.1016/j.fuproc.2021.106944

Publication date
2021

Document Version
Final published version

Published in
Fuel Processing Technology

Citation (APA)
He, S., Goldhoorn, H. R., Tegudeer, Z., Chandel, A., Heeres, A., Liu, C., Pidko, E., & Heeres, H. J. (2021). Catalytic conversion of glycerol to bio-based aromatics using H-ZSM-5 in combination with various binders. *Fuel Processing Technology*, *221*, Article 106944. https://doi.org/10.1016/j.fuproc.2021.106944

Fuel Processing Technology 221 (2021) 106944

Contents lists available at ScienceDirect

Fuel Processing Technology

journal homepage: www.elsevier.com/locate/fuproc

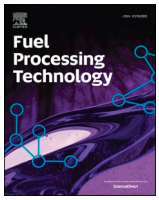

Research article

Catalytic conversion of glycerol to bio-based aromatics using H-ZSM-5 in combination with various binders

Songbo He [a], Hero Reinder Goldhoorn [a], Zhuorigebatu Tegudeer [a], Anshu Chandel [a], Andre Heeres [b], Chuncheng Liu [c], Evgeny Pidko [c], Hero Jan Heeres [a,*]

[a] Green Chemical Reaction Engineering, Engineering and Technology Institute Groningen, University of Groningen, Nijenborgh 4, 9747 AG Groningen, the Netherlands
[b] Hanze University of Applied Sciences, Zernikeplein 11, 9747 AS Groningen, the Netherlands
[c] Inorganic Systems Engineering Group, Department of Chemical Engineering, Delft University of Technology, 2629 HZ Delft, the Netherlands

ARTICLE INFO

Keywords:
Glycerol
Aromatics
BTX
H-ZSM-5
Binders

ABSTRACT

The use of H-ZSM-5 with various binders (Al_2O_3, SiO_2, and kaolinite, 10 wt% on catalyst formulation) for the catalytic conversion of glycerol to bio-based aromatics (GTA) was investigated in a continuous bench-scale unit at a pyrolysis temperature of 450 °C, catalytic upgrading temperature of 500 °C, WHSV of pure glycerol of 1 h^{-1}, and atmospheric pressure, and their performance was compared to H-ZSM-5 (SiO_2/Al_2O_3 molar ratio of 28). The latter gave a peak BTX carbon yield of ca. 31.1C.%, a life-time of ca. 220 min, and a total BTX productivity of ca. 312 mg BTX g^{-1}H-ZSM-5. The introduction of binders affects catalyst performance, which is the most profound and promising for the H-ZSM-5/Al_2O_3 catalyst. It shows a prolonged catalyst life-time of ca. 320 min and a higher total BTX productivity of ca. 518 mg BTX g^{-1}H-ZSM-5, compared to the H-ZSM-5 without a binder. Catalyst characterization studies show that the addition of the binder does not have a major effect on the specific surface area, total pore volume, and total acidity. Other relevant properties were affected, though, such as micropore volume (SiO_2), a reduced Brønsted acidity (Al_2O_3, and SiO_2), and reduced crystallinity (SiO_2). Coke formation causes severe catalyst deactivation, ultimately leading to an inactive catalyst for BTX formation. Catalyst characterization studies after an oxidative regeneration showed that the textural properties of the regenerated catalysts were close to those of the original catalysts. However, some dealumination of H-ZSM-5 occurs, resulting in decreased crystallinity and acidity, causing irreversible deactivation, which needs attention in future catalyst development studies.

1. Introduction

The use of cost-effective and non-food biomass is key for the development of biobased and circular economies. Crude glycerol, a major co-product from the bio-diesel industry that is available in large quantities (estimated to reach over 4 million tons in 2025 globally [1]), is considered an attractive feedstock for biofuels and bio-based chemicals [2]. Examples are the conversion to value-added chemicals such as 1,3-propanediol by fermentation and acrolein by dehydration [3]. Another example is the catalytic conversion of glycerol to bio-based aromatics such as benzene, toluene, and xylenes (abbreviated as BTX) [4] which has been demonstrated in a pilot-scale unit since 2019 [5]. The catalytic conversion of glycerol to aromatics (GTA) may be carried out using a catalytic pyrolysis approach, either in-situ [6] or ex-situ [4,7]. Typically acidic H-ZSM-5-based catalysts [8] are used, located either in the pyrolysis section (in-situ) or in the catalytic upgrading section after pyrolysis (ex-situ). BTX formation is inevitably associated with H_2O formation [7]) in the form of steam under pyrolysis conditions (e.g., 400–550 °C) by dehydration of glycerol and the intermediate oxygenates [9]. The long-time exposure of H-ZSM-5 under steam is known to cause dealumination of the framework [10], leading to an irreversible deactivation of the catalysts for GTA. This effect is prominently visible after a few cycles of reaction-regeneration when using either crude glycerol [4] or pure glycerol [7]. Besides, coke formation is severe, predominately in the micro-pores of H-ZSM-5 [11], resulting in reversible catalyst deactivation. As such, the H-ZSM-5-based catalysts generally show a short catalyst life-time of a few hours. Coke may be removed from the used catalyst by an oxidative regeneration [4,7,12–14].

Tailoring of the H-ZSM-5 structure, e.g., by metal modification or introducing intra-mesoporosity, could be an option to increase catalyst

* Corresponding author.
E-mail address: h.j.heeres@rug.nl (H.J. Heeres).

https://doi.org/10.1016/j.fuproc.2021.106944
Received 3 May 2021; Received in revised form 15 June 2021; Accepted 16 June 2021
Available online 1 July 2021

life-time for GTA. For instance, Xiao et al. [14–17] reported that a hierarchical H-ZSM-5 catalyst containing both micro-and mesopores (life-time of ca. 15 h [15]) and an Sn-modified H-ZSM-5 catalyst (life-time of ca. 10 h [14]) showed considerably longer life-time than an un-modified H-ZSM-5 with only micropores (life-time of ca. 5 h). Other metals, e.g., Ag (life-time of ca. 7 h) and Ni (life-time of ca. 6 h), have also been studied, showing an increased BTX yield as well [14].

Another approach could be the use of a binder, analogous to the H-ZSM-5 based catalyst used in large scale zeolite-based processes like hydrocarbon cracking in FCC-type units [12,18]. These catalysts consist of an active phase (viz., a zeolite) and auxiliary components (e.g., binder and modifier) [19]. Alumina, silica, and clays (e.g., kaolinite and bentonite) are well-known examples of binders. These are generally not inert [20] and may also be involved and act as catalysts for certain reactions (e.g., pre-cracking) [21]. Binders are typically used to i) improve the mechanical, textural, and thermal properties, ii) act as a scavenger for catalyst poisons, and iii) reduce/modify coking characteristics of the catalyst [22].

Research on binder effect on the activity and product selectivity of ZSM-5-based catalysts is limited, though some examples are known, like the aromatization of propane [20] and methanol [23], the ex-situ catalytic pyrolysis of biomass (wheat straw [24]), transalkylation of aromatics [25], and the conversion of methanol to olefins [26]. Alumina is the most widely used binder, which provides mesopores and Lewis acid sites [23] and may also lead to additional Brønsted acid sites due to Al migration [27,28]. Non-acidic silicas have also been applied and may be incorporated into the zeolite [19], lowering the Brønsted acidity for SiO_2-bonded H-ZSM-5 [26]. Kaolinite is a typical clay, and among the available clays, the most commonly used as it may form an outer layer on the zeolite due to phase changes during preparation [27,28].

For GTA, only the use of bentonite as a binder has been reported using glycerol [29], glycerol/methanol (55/45 wt%) [29], and crude glycerol [4] as the feed. Compared to ZSM-5, the ZSM-5/bentonite catalysts showed similar BTX yields but a higher selectivity to benzene at the expense of xylenes [4]. Besides, fewer poly-aromatics were formed over the ZSM-5/bentonite catalysts, particularly when using catalysts with higher bentonite intakes [29]. However, irreversible deactivation of ZSM-5/bentonite catalyst occurred when performing 11 cycles of reaction-regeneration, most likely related to collapse of the bentonite structure and the exchange of protons of H-ZSM-5 with the cations of bentonite [4]. As such, an extended binder study for the conversion of glycerol to BTX is of high interest to identify improved binders and to get a better understanding of the effect of binders on catalyst perfromance.

In this contribution, the effect of commonly used binders (Al_2O_3, SiO_2, and kaolinite) on catalyst performance for GTA (BTX yield, BTX selectivity, catalyst life-time, total BTX productivity, and turnover number (TON)) over shaped H-ZSM-5 catalysts is provided and the results are rationalized by considering relevant catalyst characteristics (structure, porosity, crystallinity, and acidity). Also, the used catalysts were characterized in detail to obtain insights into deactivation pathways. Finally, the regenerated catalysts were also characterized after an oxidative regeneration in the air to determine their potential for catalyst recycling.

2. Experimental

2.1. Materials

H-ZSM-5 with SiO_2/Al_2O_3 molar ratio of 28 (abbreviated as H-ZSM-5 (28)), boehmite, kaolinite, and SiO_2 were supplied in the powder form by Yangzhou Baisheng Catalyst Co., Ltd., PR China. All the analytical grade chemicals such as glycerol, tetrahydrofuran, ethanal, and *n*-nonane, were supplied by Sigma-Aldrich. The gases (e.g., N_2, 99.995% purity) and liquid N_2 and Ar were supplied by Linde.

2.2. Catalyst preparation

The H-ZSM-5/binder catalysts were prepared using a Caleva Multi Lab mini mixer/extruder (CML, Caleva Process Solutions Limited, England). The components (9 g H-ZSM-5 and 1 g binder) and mili-Q water (4.3–5.5 g H_2O, adjusted according to the water absorbability of the powder), were mixed in the mixer for ca. 5 min and then fed to the extruder to obtain extrudates with a diameter of ca. 2 mm and about 5–10 cm length (Fig. S1). The extrudates were placed in an oven (LT 9/11/P330, Nabertherm GmbH) using Haldenwanger porcelain crucibles (Fisher Scientific Nederlands) and dried at 110 °C for 12 h, heated to 600 °C with a heating rate of 1 °C min^{-1}, calcined at 600 °C for 8 h, and then cooled to 25 °C with a cooling rate of 1 °C min^{-1}. The samples were crushed using an agate mortar and pestle (IDL GmbH & Co. KG) and sieved using analytical sieves (Linker Industrie-Technik GmbH) to obtain catalyst particles with particle sizes between 300 and 500 μm for catalyst testing. In total, three H-ZSM-5/binder catalysts were prepared, H-ZSM-5/Al_2O_3 (90/10 wt%), H-ZSM-5/SiO_2 (90/10 wt%), and H-ZSM-5/kaolinite (90/10 wt%). Besides, the individual H-ZSM-5, Al_2O_3, SiO_2, and kaolinite particles were also prepared using the same procedure as for the H-ZSM-5/binder catalysts. The seven catalysts were stored in a vacuum desiccator (BEL-ART - SP Scienceware & HB Instruments) containing silica gel (Fisher Scientific Nederlands).

2.3. Catalytic conversion of glycerol to aromatics

The conversion of pure glycerol (>99.5% purity) to aromatics was performed in a bench-scale unit (Fig. S2), which has been designed and optimized for pure glycerol conversion over H-ZSM-5-based catalysts [7]. The unit consists of a glycerol feeding system, a vaporization/mixing device (for generating gaseous glycerol/N_2), a pyrolysis reactor filled with quartz wool (for thermal pyrolysis of glycerol), followed by a fixed bed reactor loaded with catalysts (for catalytic upgrading glycerol pyrolysis vapor), and a condenser/gas-liquid separator (for collecting gas and liquid products). The experiments for all the 7 catalysts were performed in duplicate at a pyrolysis reactor temperature of 450 °C, catalytic upgrading reactor temperature of 500 °C, atmospheric pressure, N_2 flow of 1.8 ml min^{-1}, catalyst loading of 1 g, and WHSV of pure glycerol of 1 h^{-1}. These conditions were selected based on previous research in our group [7]. The liquid products were collected every 20 min. The experiments were performed continuously until severe catalyst deactivation, which is evident from the formation of a single-phase liquid product instead of two separate liquids [7].

2.4. Catalyst regeneration

After a certain TOS, the feeding of glycerol was stopped, the reactor was cooled to room temperature under N_2 and the used catalyst was taken from the reactor for an oxidative regeneration procedure in air. For this purpose, the sample was placed in an oven (as used for catalyst calcination), which was heated to 680 °C with a heating rate of 1 °C min^{-1} and then was maintained at 680 °C for 12 h, followed by cooling to 25 °C with a cooling rate of 1 °C min^{-1}.

2.5. Liquid product analysis

The liquid product collected during a time interval of 20 min consisted of two separate layers: an aqueous and an organic phase. The combined layers were mixed with a stock solution containing ca. 10.000 ppm *n*-nonane (an internal standard) in THF to obtain a single-phase sample, which was analyzed using an HP 6890/5973 GC–MS (Hewlett-Packard) for qualification and an HP 5890 GC-FID (Hewlett-Packard) for quantification. Both GCs were equipped with an Rtx-1701 column (30 m × 0.25 mm × 0.25 μm, Restek). The carbon yields of aromatics and the carbon selectivity for the individual BTX components were calculated using Eqs. (1)–(2). The total BTX productivity and

turnover number (TON) of the catalysts are defined in Eqs. (3)–(4).

$$\text{Carbon yield}\ (\%) = \frac{\text{mol of carbon in product}}{\text{mol of carbon in the glycerol feed}} \times 100 \quad (1)$$

$$\text{Carbon selectivity for the individual BTX}\ (\%) = \frac{\text{mol of carbon in the individual BTX component}}{\text{mol of carbon in total BTX formed}} \times 100 \quad (2)$$

$$\text{Total BTX productivity}\left(g_{BTX}/g_{catalyst}\right) = \frac{\text{weight of total BTX produced}}{\text{weight of catalyst loaded in the reactor}} \quad (3)$$

$$\text{TON}\left(mol_{BTX}/mol_{acid\ sites}\right) = \frac{\text{mol of total BTX produced}}{\text{mol of acid sites on fresh catalyst}} \quad (4)$$

2.6. Catalyst characterization

The fresh, used, and regenerated catalysts were characterized by physisorption using N_2 and Ar, XRD, HR-TEM-EDX, NH_3-TPD, pyridine-IR, ^{27}Al, and ^{29}Si MAS ssNMR, TG-DTG, and elemental analysis. To obtain representative samples for experimentation, the extruded catalysts were crushed using an agate mortar and pestle (IDL GmbH & Co. KG), and the thus obtained fine powders (<40 um) were characterized.

Physisorption of N_2 at 77 K and Ar at 87 K were performed on an ASAP 2420 (Micromeritics). The surface area (S_{BET}) was calculated using Brunauer-Emmett-Teller (BET) method. The pore volume (V_{pore}) was calculated according to the single point desorption at P/P_0 of ca. 0.98. The mesopore size distribution was calculated using Barrett-Joyner-Halenda (BJH) method. The micropore volume ($V_{micropore}$) and micropore size distribution were determined using the Non-Localized Density Functional Theory method (Ar@87-Zeolites, H-Form, NLDFT, Model # 251 from Micromeritics). Powder X-Ray Diffraction (XRD) patterns were obtained on a D8 Advance Powder Diffractometer with Cu Kα radiation (λ = 1.5418 A, operated at 40 kV and 40 mA) and an LYNXEYE detector (1D mode). The relative crystallinity of a sample was calculated by comparing the height of the peak at 24.37° with that for pristine H-ZSM-5 according to ASTM method D 5758-01. The high-resolution transmission electron microscopy (HR-TEM) images were taken on a Tecnai T20 cryo-electron microscope (FEI) equipped with a Gatan model 626 cryo-stage operating at an accelerating voltage of 200 keV. Dispersive X-ray (EDX) analyses were performed on an X-Max T80 SDD detector (Oxford). Temperature-programmed desorption of ammonia (NH_3-TPD) was performed on an AutoChem II (Micromeritics) using a thermal conductivity detector. The catalysts were pretreated at 550 °C by He and subsequently, ammonia was fed to the system at 100 °C using a mixture of NH_3/He (1.0 vol%). The pyridine-IR measurements were carried out on a Nicolet 6700 FTIR spectrometer equipped with a tailor-made cell. The catalysts were pretreated at 400 °C under vacuum (<10^{-3} bar), followed by pyridine vapor addition at 25 °C, and evacuation at 160 °C. Magic angle spinning solid-state nuclear magnetic resonance (MAS ssNMR) was conducted on an AV-I 750 MHz spectrometer operated at 17.6 T. Thermogravimetric analysis and differential thermogravimetry (TG-DTG) were performed on a TGA5500 thermogravimetric analyzer (TA Instruments) using synthetic air. Elemental analysis for CHN was performed on a EuroEA3000 elemental analyzer (Eurovector). Analyses were carried out in duplicate and the average value is given.

3. Results and discussions

3.1. Ex-situ catalytic pyrolysis of glycerol to bio-based aromatics

The seven catalysts, including the three H-ZSM-5/binder catalysts (H-ZSM-5/Al_2O_3, H-ZSM-5/SiO_2, and H-ZSM-5/kaolinite), the benchmark H-ZSM-5 (SiO_2/Al_2O_3 molar ratio of 28), and the three binders (Al_2O_3, SiO_2, and kaolinite), were tested for the conversion of glycerol (> 99.5% purity) to BTX using an ex-situ catalytic pyrolysis approach. This involves heating the glycerol in a pyrolysis reactor followed by the catalytic upgrading of the vapors in a fixed bed reactor containing the catalyst. The experiments were performed continuously at a pyrolysis temperature of 450 °C, catalytic upgrading reactor temperature of 500 °C, atmospheric pressure, and a WHSV of glycerol of 1 h^{-1}. The liquid products were collected every 20 min and the experiments were performed in duplicate. The total BTX yield and the yield of the individual BTX components versus TOS are shown in Fig. 1 (on a carbon basis) and S3 (on a weight basis). In each subfigure, the data are given for H-ZSM-5, the binder, and the H-ZSM-5/binder catalyst.

Under thermal pyrolysis conditions (without a catalyst), glycerol is partly converted to a variety of oxygenates (e.g., acetaldehyde and acrolein) [7]. When the catalyst is present (and active), aromatic hydrocarbons like BTX, higher substituted benzenes (e.g. isomeric trimethyl-benzenes) and (mono- and di-substituted)-naphthalenes) are the sole products, see Fig. S4 and Tables S1-S7.

For the catalytic pyrolysis of glycerol, a typical volcano-type plot for the total BTX yield versus times on stream (TOS) is observed in all cases. At low TOS, the carbon yield is rather low (e.g., only 3.2 ± 1.6C.% over H-ZSM-5, Fig. 1), and most likely related to the start-up of the reaction in the continuous set-up. Subsequently, a steady-state period with a relatively stable BTX yield is observed for a few hours, the exact time depending on the type of catalyst (Fig. 1). At this window of TOS's and the prevailing process conditions, glycerol conversion is quantitative. The peak yield of all catalysts is given in Table 1. As an example, a peak total BTX yield of ca. 31.1 ± 4.1C.% (on a carbon basis, 14.1 ± 2.5 wt% on a weight basis) was obtained over the H-ZSM-5 catalyst. At prolonged TOS, glycerol conversion is not quantitative anymore and a considerable drop in BTX yield is observed, and this is ascribed to severe catalyst deactivation. To quantify catalyst deactivation, the term catalyst life-time (Table 1) is used, which is defined as the TOS at which BTX formation is below 2C.%. (Fig. 1). Besides peak yield and life-time, it is also of interest to determine the cumulative BTX yield, which is expressed in terms of BTX productivity per g catalyst or per gram H-ZSM-5 in the catalyst formulation (Table 1). For H-ZSM-5 alone, it is 312 mg. g^{-1}H-ZSM-5.

In the absence of H-ZSM-5, the three binders (Al_2O_3, SiO_2, and kaolinite) show very low BTX yields (Fig. 1) with peak yields between 1.6 and 4.3C.% (Table 1). As such, the binders alone have a certain activity, though by far lower than for the H-ZSM-5 catalyst (31.1C.%).

Binder effects on catalyst performance are visible, though the extent is a function of the type of binder. When using SiO_2, the BTX versus TOS profile is very similar to the one for H-ZSM-5 only (Fig. 1-ii). However, when compensating for the fact that the H-ZSM-5/SiO_2 catalyst contains less H-ZSM-5 (10% less), a slightly higher BTX productivity (362 mg BTX g^{-1}H-ZSM-5, Table 1) is calculated (H-ZSM-5: 312 mg BTX g^{-1}H-ZSM-5. As such, the effect of SiO_2 addition is minor. Comparable performance was found for the kaolinite based catalyst, though catalyst life-time seems somewhat longer than for SiO_2.

The BTX versus TOS curves for the catalyst with Al_2O_3 deviates considerably from H-ZSM-5 alone (Fig. 1), and the other H-ZSM-5/binder combination. The BTX peak yield in the steady-state period is slightly reduced (Fig. 1-i), though the catalyst life-time is prolonged considerably to 320 min (versus 220 for the H-ZSM-5 benchmark, Table 1), giving a productivity at least 50% higher than for H-ZSM-5 alone.

The selectivity for the individual BTX components for H-ZSM-5 and the H-ZSM-5/binder catalysts is shown in Fig. 2. Overall, the trends for the selectivity versus time on stream are similar and show that the benzene selectivity is reduced at longer TOS, whereas more xylenes, and particularly m,p-xylenes are formed. However, compared to H-ZSM-5, the three H-ZSM-5/binder catalysts show a considerably lower benzene selectivity and higher toluene and xylenes selectivity at short times on

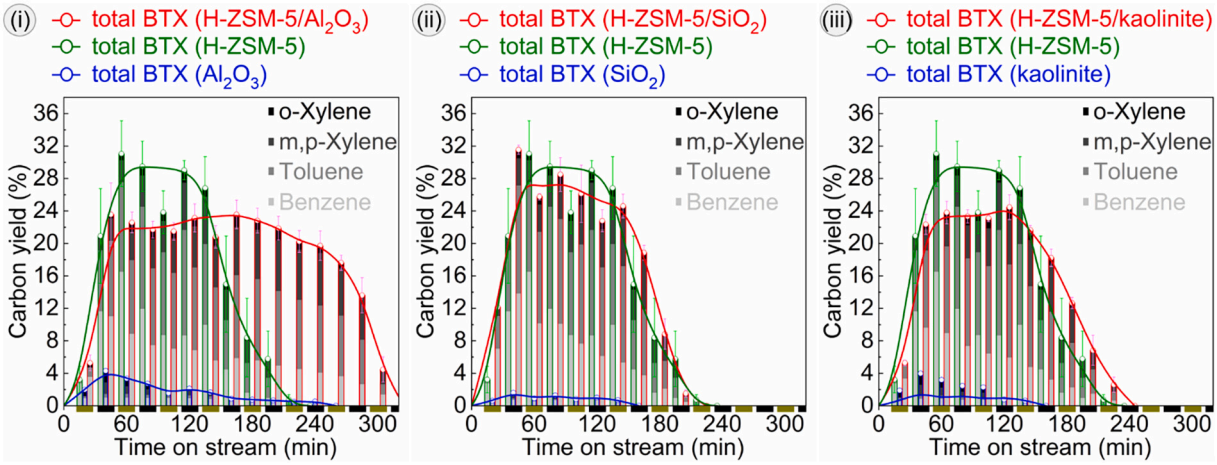

Fig. 1. Carbon yields of the total and individual BTX versus TOS over H-ZSM-5, the three binders, and the three H-ZSM-5/binder catalysts. Reaction conditions: pyrolysis temperature of 450 °C, catalytic upgrading temperature of 500 °C, atmospheric pressure, N_2 flow of 1.8 ml min^{-1}, catalyst (300–500 μm, 1 g), and a WHSV of glycerol of 1 h^{-1}.

Table 1
Catalyst performance indicators for the conversion of glycerol to BTX.

	Peak yield of total BTX		Life-time of 1 g catalyst (min)	Total BTX productivity over the catalyst life-time		TON	
	on mass basis (wt%)	on carbon basis (C.%)		(mg BTX g^{-1} catalyst)	(mg BTX g^{-1}H-ZSM-5)	(mol BTX mol^{-1} Brønsted acid sites)[a]	(mol BTX mol^{-1} total acid sites)[b]
H-ZSM-5	14.1	31.1	220	312	312	4.9	2.5
Al_2O_3	2.3	4.3	–	34	–	–	1.1
SiO_2	0.8	1.6	–	11	–	–	1.5
Kaolinite	2.1	4.0	–	26	–	–	1.4
H-ZSM-5/ Al_2O_3	11.8	23.6	320	466	518	10.1	4.1
H-ZSM-5/SiO_2	14.9	31.6	220	326	362	6.8	2.8
H-ZSM-5/ Kaolinite	12.2	24.5	240	302	336	4.9	2.5

Acid sites were measured by [a]Pyridine-IR and [b]NH_3-TPD.

stream (TOS < 1 h, Fig. 2). In the steady-state regime, also some remarkable differences between H-ZSM-5 and the H-ZSM-5/binder catalysts are found. Of interest is the observation that the reduction in benzene selectivity versus TOS is by far more pronounced for H-ZSM-5 than for the H-ZSM-5/binder catalysts. Also remarkably is a constant carbon selectivity to toluene (ca. 43–45%) and o-xylene (ca. 4–6%) in the steady-state period (Fig. 2). Thus, we can conclude that in the steady-state period, benzene selectivity is reduced, toluene selectivity is about constant, and m,p-xylene selectivity is increased. This change in chemoselectivity is likely related to changes in catalyst acidity and microporosity during TOS [11] and will be discussed in more detail after the catalyst characterization studies.

3.2. Characterization of the fresh catalysts

H-ZSM-5, the three binders, and the H-ZSM-5/binder catalysts were characterized by various techniques including HR-TEM-EDX, N_2, and Ar physisorption, XRD, NH_3-TPD, pyridine-IR, and ^{27}Al and ^{29}Si MAS ssNMR, to get insights into the effect of binders on catalyst characteristics. An overview of all relevant data is given in Table 2. In the following, the main features of the fresh catalysts will be discussed.

3.2.1. HR-TEM-EDX

The HR-TEM image of H-ZSM-5 (Fig. S5-left column) shows the ordered lattice fringe, indicating its highly crystalline structure and in line with the literature data [7,30]. The morphology of the three binders is different from H-ZSM-5 (Fig. 3-left column), which enables to distinguish the particles of H-ZSM-5 and those of the binders in the H-ZSM-5/binder formulation (Fig. 3-middle column). The TEM images of the H-ZSM-5/binder catalysts show that the binder may cover the H-ZSM-5 particles (e.g., Fig. 3-middle column-ii) and also connect individual H-ZSM-5 particles (e.g., Fig. 3-middle column-i-iii). This is also confirmed by EDX mapping (Fig. 3-right column), showing a non-uniform distribution of the elements of the binder in the H-ZSM-5/binder catalyst (Fig. 3-middle column-i-iii), which is different from the homogeneously distributed Al and Si in H-ZSM-5 (Fig. S5-right column). This non-homogeneous distribution of H-ZSM-5 and the binder might be related to differences in particle sizes and is commonly observed for H-ZSM-5/binder systems [27,28].

3.2.2. N_2 and Ar physisorption

Both physisorption of N_2 (at 77 K) and Ar (at 87 K) experiments were performed for a comprehensive determination of the textural properties [31]. N_2 adsorption-desorption isotherms of H-ZSM-5 (Fig. 4-A-b) show the combination of Type I and Type IV isotherms [32], indicating the presence of micro-pores and inter-crystalline voids of H-ZSM-5 [32,33]. The latter is represented by the BJH mesopore size distribution (meso-PSD) of H-ZSM-5 (Fig. 4-B-b) measured by N_2 physisorption using the Barrett-Joyner-Halenda method. Here a maximum in the distribution is found at ca. 3.8 nm, which is in agreement with literature data [4,34]. The micro-pore structure is well reflected by the NLDFT micro-pore size distribution (micro-PSD) of H-ZSM-5 (Fig. 4-C-b) determined by Ar physisorption using the non-localized density functional theory method. It shows a micro-PSD centered at ca. 0.51 nm (close to the reported

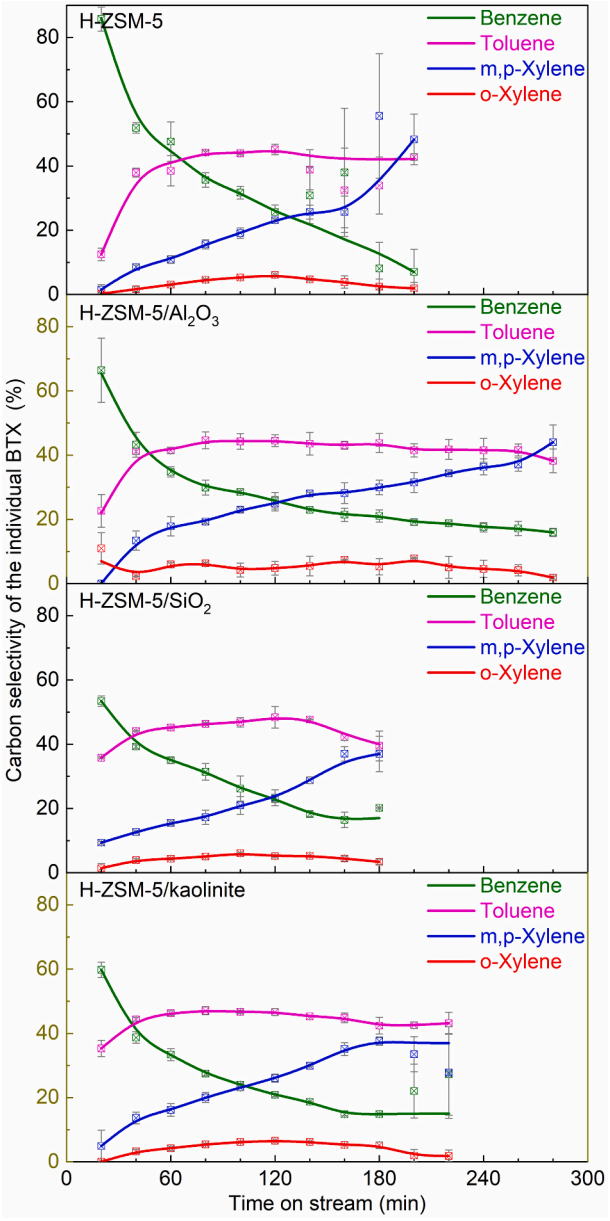

Fig. 2. Carbon selectivity of the individual BTX versus TOS over H-ZSM-5 and the three H-ZSM-5/binder catalysts. Reaction conditions: pyrolysis temperature of 450 °C, catalytic upgrading temperature of 500 °C, atmospheric pressure, N_2 flow of 1.8 ml min^{-1}, catalyst (300–500 μm) loading of 1 g, and WHSV of glycerol of 1 h^{-1}.

values of 0.52–0.55 nm [7,35]) with two artifacts [36] centered at ca. 0.92 nm and <0.44 nm. The specific surface area (S_{BET}, 353 m^2 g^{-1}), total pore volume (V_{pore}, 0.19 cm^3 g^{-1}), and micropore volume ($V_{micropore}$, 0.21 cm^3 g^{-1}) of the H-ZSM-5 (28) used in this study (Table 2) are close to those reported for H-ZSM-5(23) [4,7].

The N_2 adsorption-desorption isotherms for the three binders are shown in Fig. 4. Al_2O_3 shows typical features of a Type IV isotherm (Fig. 4-i-A-a) [32], attributed to the adsorption in the mesopores [37] with a meso-PSD centered at ca. 5.5 nm (Fig. 4-i-B-a). SiO_2 and kaolinite show Type II isotherm (Fig. 4-ii and iii-A-a) [32] and contain macropores centered at ca. 50 nm (Fig. 4-ii and iii-B-a), in agreement with the literature data for silica microspheres [38] and nature kaolin [39].

Compared to H-ZSM-5, the three H-ZSM-5/binder catalysts show slightly lower S_{BET} values (Table 2), related to the dilution of H-ZSM-5 by the three binders with lower S_{BET} values [28]. As expected, the H-

Table 2
Characterizations of fresh, used and regenerated catalysts.

	S_{BET}[a] (m^2 g^{-1})			V_{pore}[a] (cm^3 g^{-1})			NLDFT $V_{micropore}$[b] (cm^3 g^{-1})			Acidity[c] (μmol pyridine g^{-1} sample)					Acidity[d] (μmol NH_3 g^{-1} sample)			Relative crystallinity[e]		Carbon content[f] (wt%)	Coke content[g] (wt%)	T_M of DTG[g] (°C)
	fresh	used	regenerated	fresh	used	regenerated	fresh	used	regenerated	Brönsted acid (B)	Lewis acid (L)	B + L	B/L		fresh	used	regenerated	fresh	regenerated			
H-ZSM-5	353	6	282	0.19	0.01	0.16	0.21	0.02	0.20	714	143	857	5.0		1387	363	670	100	77	8	8	590
Al_2O_3	171	21	134	0.28	0.04	0.27	–	–	–	–	–	–	–		332	204	332	–	–	21	21	512
SiO_2	135	101	125	1.1	0.76	0.81	–	–	–	–	–	–	–		81	37	54	–	–	9	10	540
Kaolinite	116	58	105	0.42	0.29	0.41	–	–	–	–	–	–	–		198	88	121	–	–	14	17	525
H-ZSM-5/Al_2O_3	336	10	312	0.23	0.03	0.23	0.23	0.03	0.27	503	129	632	3.9		1238	92	629	96	81	15	15	585
H-ZSM-5/SiO_2	329	7	300	0.28	0.09	0.27	0.16	0.03	0.23	526	118	644	4.4		1286	137	643	83	70	10	9	590
H-ZSM-5/Kaolinite	297	13	278	0.22	0.04	0.20	0.23	0.03	0.20	668	214	882	3.1		1318	109	652	105	62	10	13	574

[a] N_2 adsorption-desorption at 77 K.
[b] Ar adsorption-desorption at 87 K.
[c] Pyridine-IR.
[d] NH_3-TPD.
[e] XRD.
[f] CHN elemental analysis.
[g] TG-DTG.

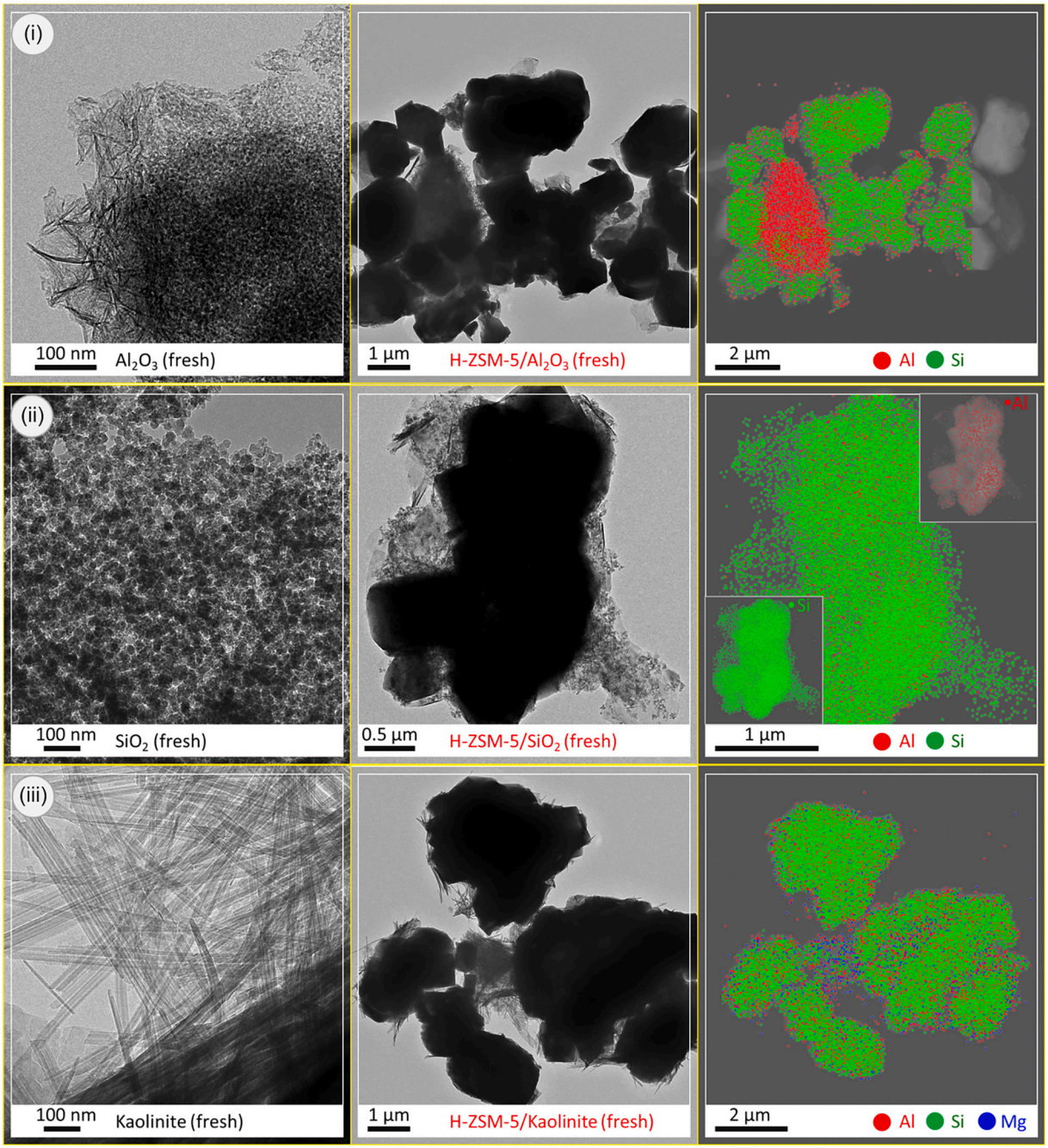

Fig. 3. HR-TEM images of the three binders (left), TEM images (middle), and elemental maps (right) of the three H-ZSM-5/binder catalysts.

ZSM-5/binder catalysts show a slightly increased V_{pore} (Table 2), attributed to the meso- or macro-porosity of the corresponding binders. Nevertheless, the experimental data of S_{BET} and V_{pore} for the three H-ZSM-5/binder catalysts are very close to the theoretical values calculated using the composition of the catalyst and the contribution of the individual components (Table S8). These results indicate that specific surface area and total pore volume are hardly affected by introducing a small amount of binders (10 wt%). This is also reflected in the slight changes of the $V_{micropore}$ for H-ZSM-5/Al_2O_3 and H-ZSM-5/kaolinite catalysts (Table 2). However, the H-ZSM-5/SiO_2 catalyst shows a significantly decreased $V_{micropore}$ (0.16 $cm^3\ g^{-1}$, Table 2), most likely due to the coverage of the micropores of H-ZSM-5 [28] by the outer layer of SiO_2 as also observed by TEM-EDX (Fig. 3-middle column-ii, vide supra).

3.2.3. XRD

The XRD pattern of H-ZSM-5 (Fig. 5-b) shows two typical peaks (♥) at 2θ = ca. 7.9° and 8.9°, corresponding to the [011] and [200] planes [40] for MFI-type zeolites and also the other XRD features are in agreement with the literature [4,14,34]. The XRD patterns of the three binders are shown in Figs. S5–S7, corresponding to cubic alumina (ICDD: 00-029-0063, Fig. S6), non-crystalline silica (ICDD: 00-029-0085, Fig. S7), and calcined kaolin (Fig. S8, showing combined XRD features of kaolinte, illite, and quartz, etc. [41]). In general, the intensity of the XRD peaks for the three binders is considerably lower than for H-ZSM-5 (Figs. 5-i-iii, a vs. b), indicating that H-ZSM-5 has a by far higher crystallinity than the binders, in agreement with the HR-TEM results (vide supra). As such, the three H-ZSM-5/binder catalysts mainly show the XRD features of H-ZSM-5 (Fig. 5-i-iii, c). This observation was also reported for an H-ZSM-5/Al_2O_3 catalyst with 40 wt% of Al_2O_3 [42]. The

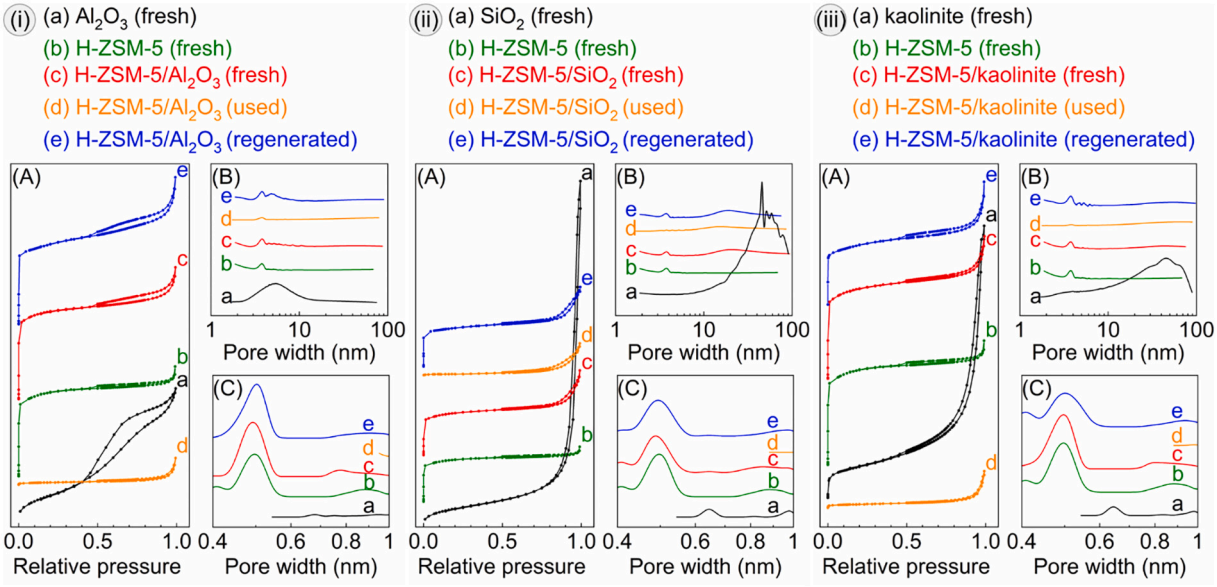

Fig. 4. N_2 adsorption-desorption isotherms (A), BJH meso-pore size distribution (B), and NLDFT micro-pore size distribution (C) of H-ZSM-5, the three binders, and the three H-ZSM-5/binder catalysts.

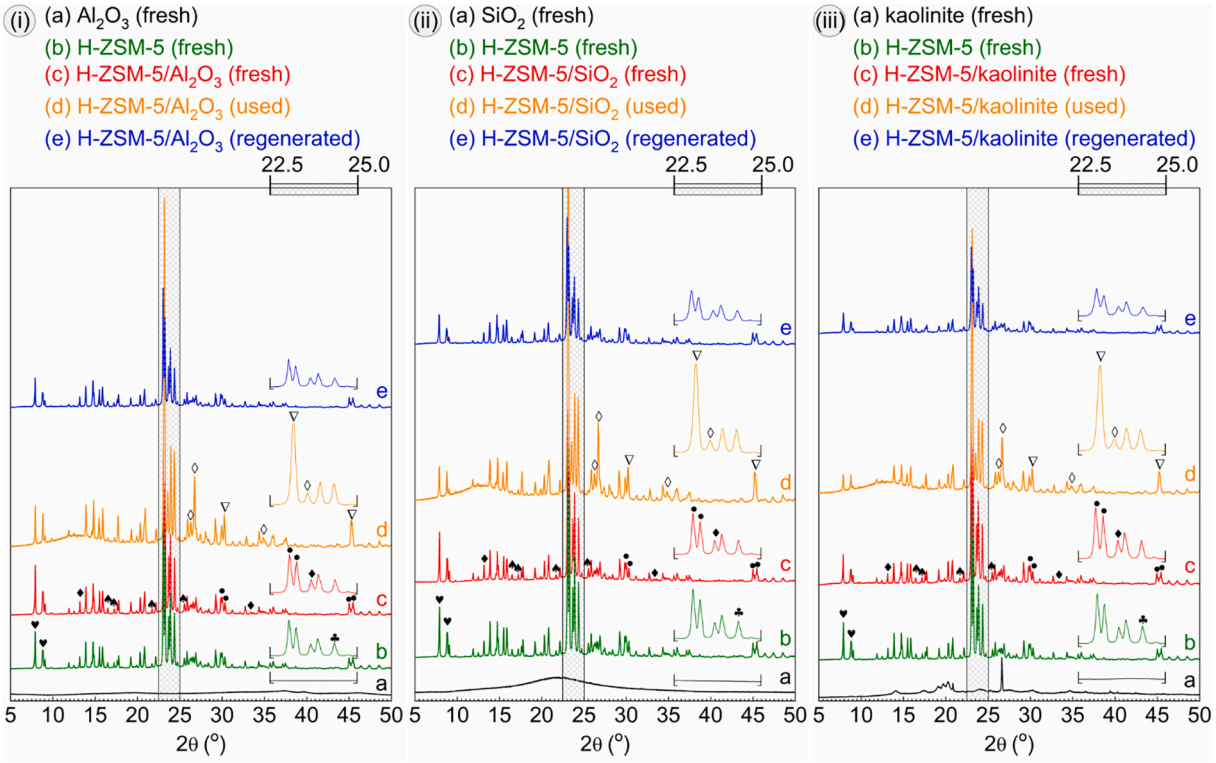

Fig. 5. XRD patterns of H-ZSM-5, the three binders, and the three H-ZSM-5/binder catalysts.

relative crystallinity of the H-ZSM-5/binder catalysts was calculated by comparing the height of the XRD peak (♣) at 2θ = ca. 24.37° with that for H-ZSM-5 and the data is given in Table 2. Compared to H-ZSM-5, the highly crystalline structure is well retained in the H-ZSM-5/Al_2O_3 and H-ZSM-5/kaolinite catalysts (relative crystallinity of 100 ± 5%, Table 2). However, a substantial decrease in relative crystallinity was found for H-ZSM-5/SiO_2 (83%, Table 2), indicating disruption of the H-ZSM-5 framework after the introduction of SiO_2.

3.2.4. NH_3-TPD and pyridine-IR

The NH_3-TPD profile of H-ZSM-5 (Fig. 6-b) shows two peaks centered at ca. 210 °C and 410 °C, in line with the literature data [7,27]. These are from weak Lewis acid, and strong Brønsted acid sites [4,40]. The total acidity is approximately 1387 μmol NH_3 g^{-1}H-ZSM-5 (Table 2). The three binders have a considerably lower total acidity (Table 2), and mainly show weak acidic sites (Fig. 6-i-iii-a). The three H-ZSM-5/binders catalysts show similar NH_3-TPD curves (Fig. 6-i-iii-c) and total acidity (Table S8). In each subfigure, the theoretical total acidity (based

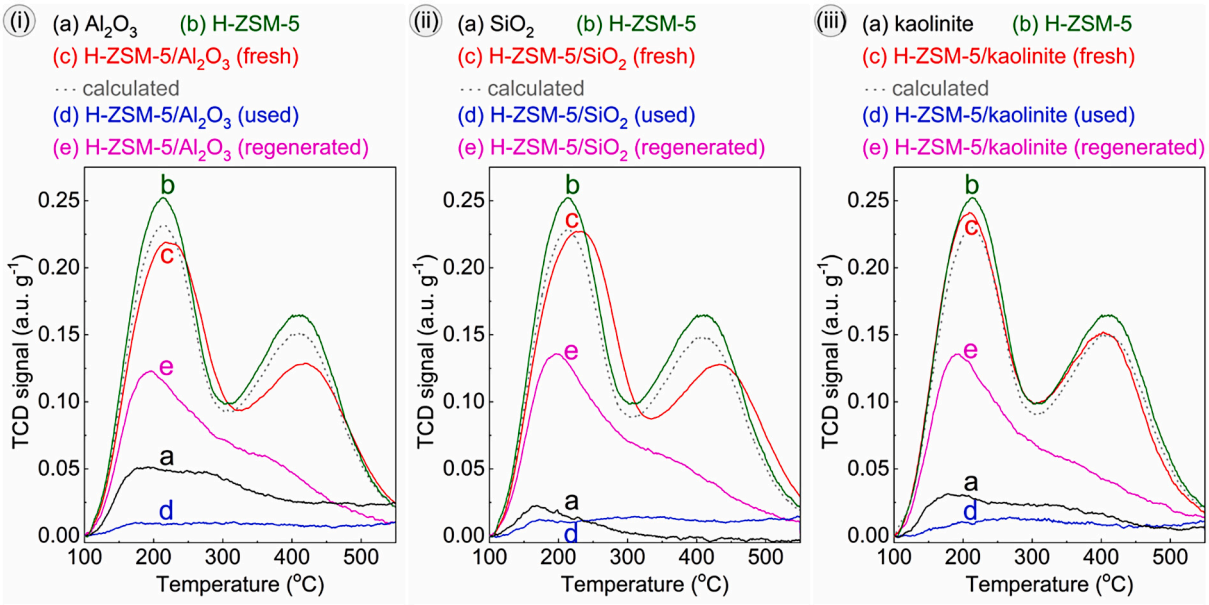

Fig. 6. NH_3-TPD profiles of H-ZSM-5, the three binders, and the three H-ZSM-5/binder catalysts.

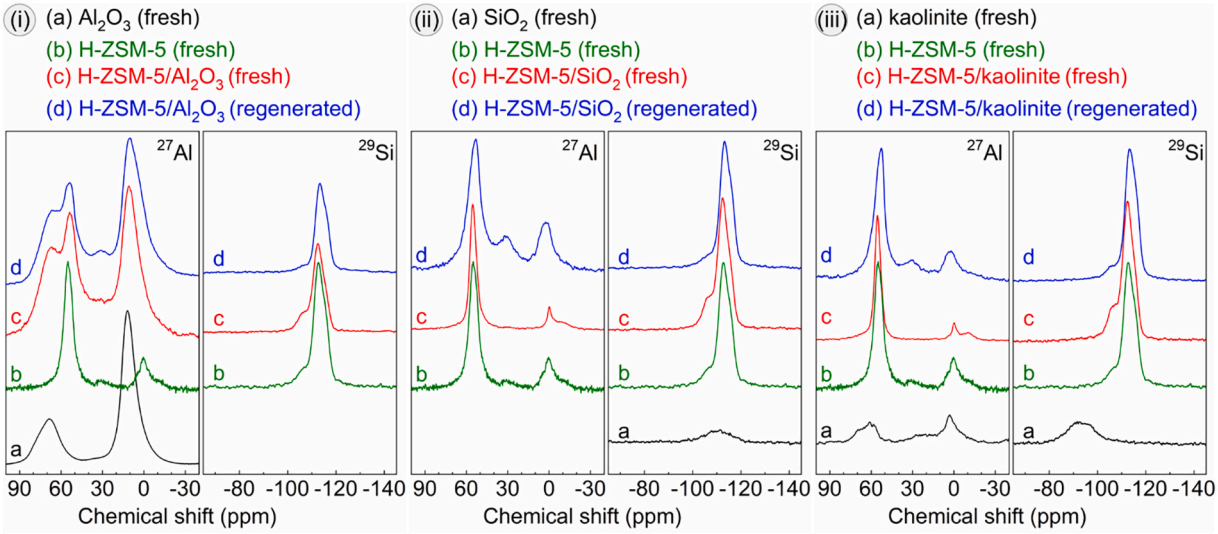

Fig. 7. ^{27}Al and ^{29}Si MAS ssNMR spectra of H-ZSM-5, the three binders, and the three H-ZSM-5/binder catalysts.

on catalyst composition and acidity of individual components) is also provided (Fig. 6-i-iii-dotted lines and Table S8) and good agreement was observed. Thus, synergic effects between the binder and H-ZSM-5 are absent, probably related to the low amount of binder used in this study (10 wt%).

Pyridine-IR analyses were performed and the spectra are shown in Fig. S9. The two bands centered at ca. 1455 cm^{-1} and 1545 cm^{-1} (Fig. S9), corresponding to the C-CN vibrations of metal-coordinated pyridine and protonated pyridine, respectively [43], were used to quantify the Lewis and Brønsted acid sites [4,17,33]. As expected, the Brønsted acidity of the H-ZSM-5/binder catalysts is lower than that of H-ZSM-5 (Table 2), due to the dilution of H-ZSM-5 with the three binders without Brønsted acidity. However, the Brønsted acidity of H-ZSM-5/Al_2O_3 and H-ZSM-5/SiO_2 is considerably lower than the theoretical one based on catalyst composition and acidity of individual compounds (Table S8). This reduction in Brønsted acidity after introducing the binders to H-ZSM-5 has been reported in the literature [26] and could be due to dealumination or neutralization by solid-state ion exchange of the H-ZSM-5 framework during catalyst preparation [26,28].

3.2.5. *^{27}Al and ^{29}Si MAS ssNMR*

Possible changes in the H-ZSM-5 framework upon the introduction of the binder were investigated by ^{27}Al and ^{29}Si MAS ssNMR analyses. The ^{27}Al MAS ssNMR spectrum of H-ZSM-5 (Fig. 7-b) shows two distinct peaks at δ = ca. 0 ppm (associated with the octahedrally coordinated extra-framework Al [44], abbreviated as EFAl) and ca. 53 ppm (attributed to the tetrahedrally coordinated framework Al [44], abbreviated as FAl), and a small peak at δ = ca. 30 ppm (related to pentahedrally coordinated extra-framework Al [45]). The latter could be from an aluminum species (e.g., $Al(OH)_2^+$) formed by the interaction of Brønsted acid sites with the EFAl migrated from the framework [7,45]. In literature, the decrease in the peak intensity of FAl [26] or an increase in the ratio of the peak intensities of EFAl and AAl (I_{EFAl}/I_{FAl}, Al method) [4,7] has been often applied to indicate the level of dealumination of the H-ZSM-5 framework. The ^{29}Si MAS ssNMR spectrum of H-ZSM-5 (Fig. 7-b) shows a sharp peak at δ = ca. -113 ppm and a small shoulder at δ = ca.

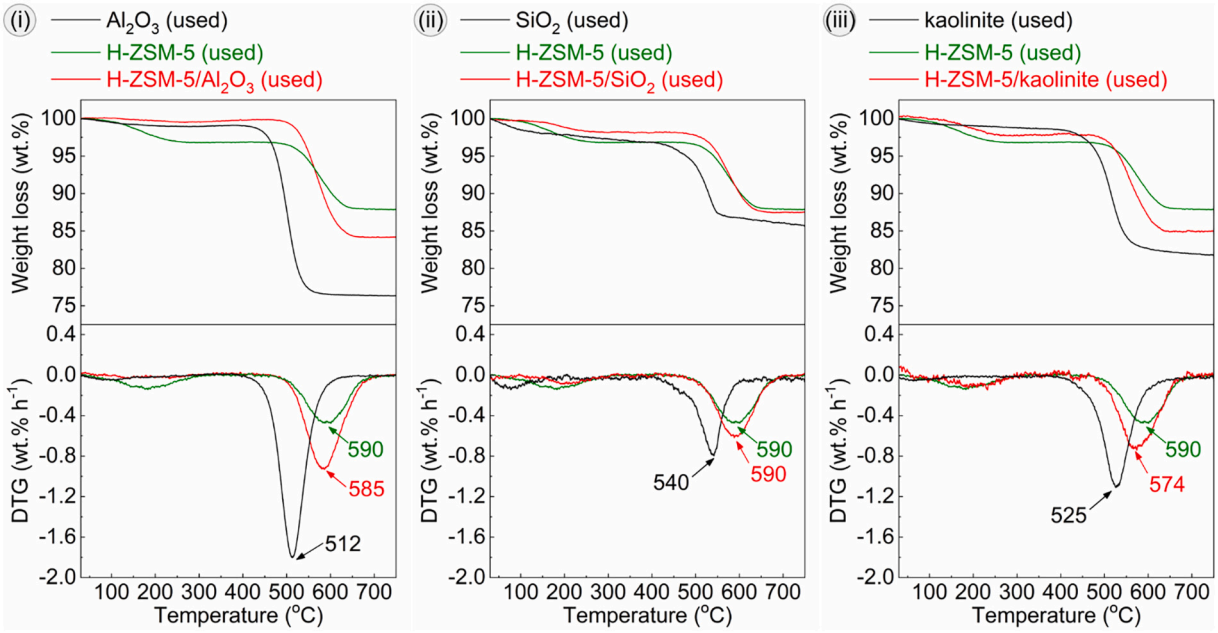

Fig. 8. TG-DTG curves of the used H-ZSM-5, the three used binders, and the three used H-ZSM-5/binder catalysts.

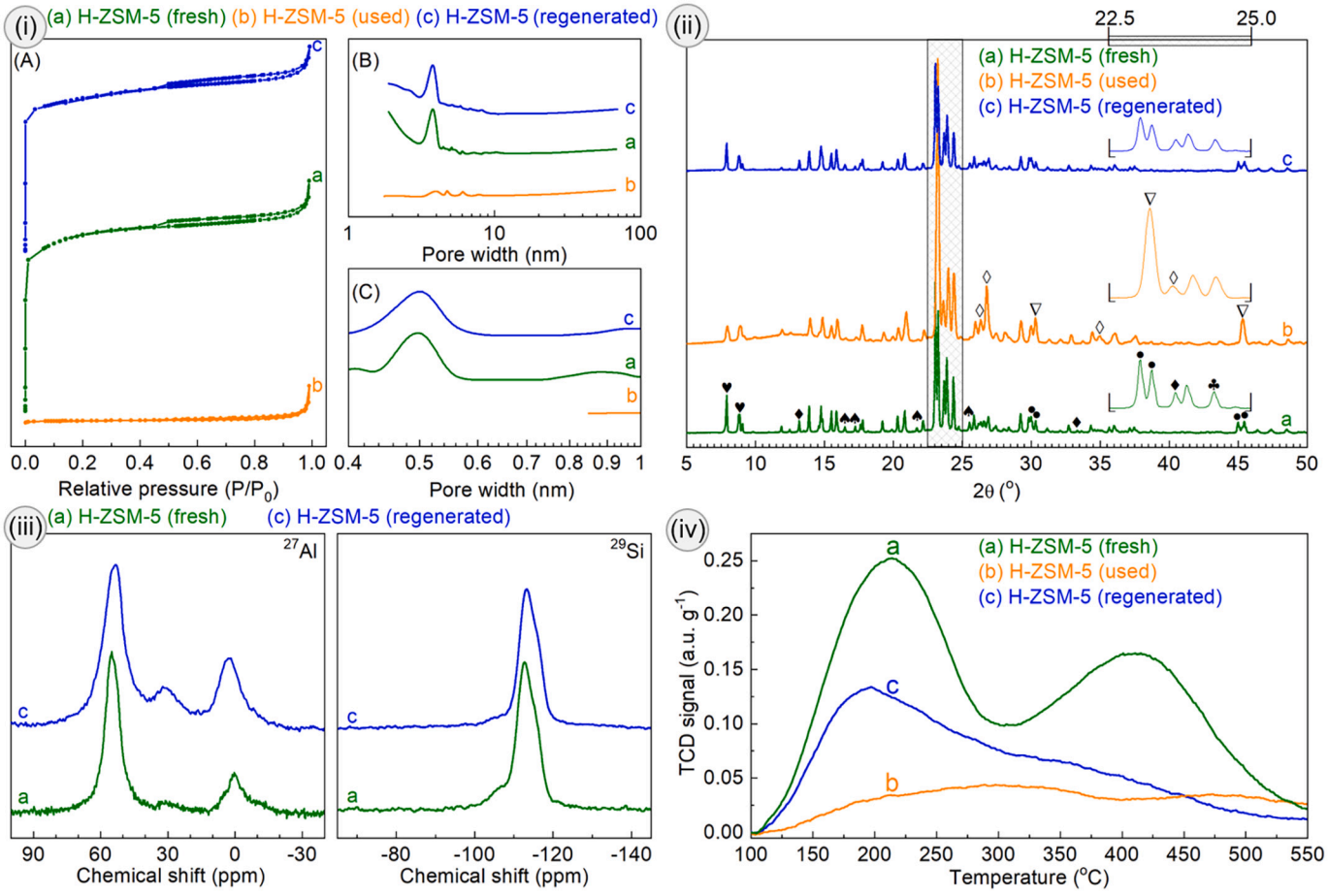

Fig. 9. (i) N_2 adsorption-desorption isotherms (A), BJH meso-pore size distribution (B), and NLDFT micro-pore size distribution (C), (ii) XRD patterns, (iii) ^{27}Al and ^{29}Si MAS ssNMR spectra, and (iv) NH_3-TPD profiles of the (a) fresh, (b) used, and (c) regenerated H-ZSM-5 catalysts.

-106 ppm, corresponding to Q4-linkage Si(4Si, 0Al) and Si(3Si, 1Al) in the framework [4,45]. The reduction of the peak intensity of Si(3Si, 1Al) or the increase of the peak intensity ratio of Si(4Si, 0Al) to Si(3Si, 1Al) ($I_{Si(4Si,\ 0Al)}/I_{Si(3Si,\ 1Al)}$, Si method) has also been used in literature as the indicator for the extent of dealumination of the H-ZSM-5 framework [7].

The binders alone also show peaks in ^{27}Al and/or ^{29}Si MAS ssNMR spectra (Fig. 7-i-iii-a), and typically overlap with those of H-ZSM-5 (Fig. 7-i-iii-c). Therefore, for quantification of extra-framework Al species after introducing the binders, the Al-method (I_{EFAl}/I_{FAl}) was applied for H-ZSM-5/SiO_2 catalyst and the Si-method ($I_{Si(4Si,\ 0Al)}/I_{Si(3Si,\ 1Al)}$) for H-ZSM-5/$Al_2O_3$ and H-ZSM-5/kaolinite catalysts. The I_{EFAl}/I_{FAl} and $I_{Si\ (4Si,\ 0Al)}/I_{Si(3Si,\ 1Al)}$ values (Table S9) show a lower amount of EFAl in the H-ZSM-5/binder catalysts compared to the H-ZSM-5 catalyst, indicating that dealumination of the H-ZSM-5 framework does not occur during the introduction of the binders. Therefore, the decreased Brønsted acidity for the H-ZSM-5/binder catalysts (vide supra) is mainly caused by the neutralization of acid sites related to the solid-state reactions of the Brønsted protons of the H-ZSM-5 framework with specific ions of the binders [26]. This was also reported previously for bentonite [4] and kaolin [46] bonded MFI zeolite-based catalysts.

Based on this extensive set of characterization data for H-ZSM-5, the three binders, and the H-ZSM-5/binder catalysts, we can conclude that:

1. The three binders, Al_2O_3, SiO_2, and kaolinite, interact with H-ZSM-5 particles, forming a connected structure (Fig. 3). The binders may form a layer covering the surface of the H-ZSM-5 particles [25,47].
2. The introduction of these binders (10 wt%) does not show a major effect on the surface area, total pore volume, and total acidity for the corresponding H-ZSM-5/binder catalysts when considering the dilution effect (Tables 2 and S1).
3. The addition of macroporous SiO_2 binder (10 wt%) to H-ZSM-5 leads to a decreased microporosity, a reduction of the crystallinity, and a lower Brønsted acidity for the H-ZSM-5/ SiO_2 catalyst (Tables 2 and S1).
4. The introduction of mesoporous alumina binder (10 wt%) has a minor effect on the microporosity and crystallinity of the H-ZSM-5/ Al_2O_3 catalyst, though the Brønsted acidity is slightly lower than anticipated (Tables 2 and S1).
5. The properties of the H-ZSM-5/kaolinite catalyst are as expected (Tables 2 and S1) based on the properties of the individual components and the amount in the formulation (10 wt% of kaolinite).

3.3. Characterization of the used catalysts

The used H-ZSM-5, the three used binders, and the three used H-ZSM-5/binder catalysts after the reaction were characterized by the same characterization techniques used for the fresh catalysts, supported by TG-DTG (Fig. 8) and CHN elemental analyses, to get insights into catalyst deactivation during the reaction.

Coking has been considered as the important factor causing catalyst deactivation for GTA and the amount of coke on the catalyst is generally analyzed by TG-DTG [4,7,11,17] or temperature-programmed oxidation (TPO) [6,13,15–18]. A TG curve of the used H-ZSM-5 (Fig. 8) shows a weight loss of ca. 8 wt%. (Table 2) at a temperature of 450–650 °C, in agreement with the result of elemental analysis showing ca. 8 wt% of carbon (Table 2). The T_M of the DTG curve (Fig. 8) is ca. 590 °C (Table 2), in line with the literature data [11]. The coke has high crystallinity, indicated by the new peaks (▽) present in the XRD pattern of the used H-ZSM-5 (Fig. 9-ii-b) compared to the fresh one (Fig. 9-ii-a). This observation implies that the coke is graphitic in nature [4,7,11]. The coke leads to a strong reduction in acidity (ca. 74%, (Fig. 9-iv-b and Table 2), surface area (S_{BET} of only 6 $m^2\ g^{-1}$, Table 2), and the micro-and meso-PSD (Fig. 9-i-b). The activity of the spent catalyst for BTX formation was negligible, and as such, the amount of coke on the spent H-ZSM-5 catalyst is defined as the maximum coke accommodation capacity of the catalyst and will be used for comparison with the H-ZSM-5/binder catalysts.

The three used H-ZSM-5/binder catalysts show similar characteristics as found for the used H-ZSM-5, viz. a significant loss in porosity (Fig. 4-i-iii-d and Table 2) and a substantial decrease in acidity (Fig. 6-i-iii-d and Table 2), as a result of coke deposition (Fig. 8 and Table 2).

The coke contents of the used H-ZSM-5/binder catalysts are a function of the binder type (Table 2). Of interest is the observation that all show a higher coke content (9–15 wt%, Table 2) than the used H-ZSM-5 catalyst (8 wt%), indicating that the H-ZSM-5/binder catalysts have a considerably higher coke accommodation capacity. This is most likely related to the meso- and macro-porosity of the binders (Al_2O_3 and SiO_2, vide supra), which have a higher coke accommodation capacity than H-ZSM-5. Support for this statement also comes from the amount of coke on the spent binders only, which are considerably higher (10–21 wt% carbon, Table 2) compared to the microporous H-ZSM-5.

Besides, the T_M of DTG curves for the used H-ZSM-5/Al_2O_3 (585 °C) and H-ZSM-5/kaolinite catalysts (574 °C) shifted to a lower temperature compared to the used H-ZSM-5 catalyst (Fig. 8-i-iii and Table 2). This means that the regeneration of the used H-ZSM-5/binder catalysts via oxidation in the air could be accomplished at relatively lower temperatures compared to H-ZSM-5 catalyst, which might cause less damage to the catalyst surface and structure after regeneration (particularly after multiple reaction regeneration cycles), causing irreversible catalyst deactivation [4,7].

3.4. Catalyst structure-performance relations

In this paragraph, the data obtained from the catalyst characterization studies will be related to the performance of the catalysts in terms of peak BTX yield and catalyst life-time.

When considering peak BTX yield in the steady-state of operation (TOS of 60–120 min, Fig. 1), it is evident that the use of a binder in low amounts (e.g., 10 wt%) does not have a positive effect on catalyst activity. When using SiO_2, the BTX-yield-TOS curves H-ZSM-5/SiO_2 are very similar to that of H-ZSM-5 (Fig. 1-ii). SiO_2 is marginally active for the conversion of the pyrolysis vapor and also for BTX formation, see the experimental BTX yield over SiO_2 alone (Fig. 1-ii and Table 1). Therefore, no obvious difference is observed for the BTX yield curves for the H-ZSM-5 catalyst and the H-ZSM-5/SiO_2 catalyst. However, for the other 2 binders, the BTX yields over the two H-ZSM-5/binder catalysts are lower than over the H-ZSM-5 catalyst (Fig. 1-i and 1-iii). When considering these differences in peak yields, this is likely not due to a dilution effect of the binders (c.f. the data in Table 1, H-ZSM-5 peak yield of 14.1 wt%, which is reduced to 11.8 wt% when using the alumina binder (10 wt%), which is lower than when considering dilution only (12.7 wt%).

A possible explanation is involvement of the binders in the reaction network for the conversion of glycerol to BTX. It is well possible that glycerol pyrolysis vapors are converted, e.g., to C_1 - C_3 oxygenates by dehydration over the binders, which is known for Al_2O_3 [48]. This also leads to coke formation in the binders, which lowers the concentration of organics in the stream for aromatization in H-ZSM-5, resulting in a lower peak BTX yield (23.6C.% over the H-ZSM-5/Al_2O_3 catalyst compared to 31.1C.% over the H-ZSM-5 catalyst, Fig. 1 and Table 1).

Remarkable differences in catalyst life-time were observed for the three H-ZSM-5/binder catalysts, and particularly for the H-ZSM-5/Al_2O_3 catalyst, which showed an extended life-time of more than 45% compared to H-ZSM-5 (Fig. 1). Catalyst life-time of H-ZSM-5-based catalyst for the GTA process is typically related to the coke formation, and it is well established that H-ZSM-5 becomes inactive for BTX formation when the coke level on the catalyst has reached a level (e.g., 8 wt %, Table 2) at which all micropores are filled with coke (Table 2). Apparently, the use of alumina as a binder has a major impact on the amount and the location of the coke in the catalyst formulation. The coke formed in the micro-pores of H-ZSM-5 may migrate to the crystallite surface [49], and further to the connected mesopores of the binder when available [4] (e.g., Al_2O_3). As such, the coking rate of the H-ZSM-5

catalysts, active for BTX formation, is reduced [25]. The mesoporous Al_2O_3 binder has a considerably higher coke accommodation capacity than microporous H-ZSM-5 (21 vs. 8 wt%, Table 2), leading to a reduced coking rate of H-ZSM-5 and, ultimately, to a prolonged catalyst life-time for the H-ZSM-5/Al_2O_3 catalyst. This significantly prolonged catalyst life-time of the H-ZSM-5/Al_2O_3 catalyst results in a high total BTX productivity of 518 mg BTX g^{-1}H-ZSM-5 and a TON of 10.1 mol BTX mol^{-1} Brønsted acid sites (Table 1). As such, Al_2O_3 is the best binder among the three binders investigated here to prepare the shaped H-ZSM-5/binder catalysts for GTA. This finding also confirms that an H-ZSM-5/binder catalyst with a proper binder (e.g., Al_2O_3) can match or exceed the performance of hierarchical H-ZSM-5 catalysts [15,17] for GTA, in agreement with the literature [26].

3.5. Characteristics of the regenerated catalysts

Besides coke formation, other relevant characteristics of the catalysts may also be affected (e.g., porosity, crystallinity, and acidity, Table 2) and have an impact on the extent of catalyst deactivation. Coke formation is typically considered as reversible deactivation, as it has been shown that the coke may be removed effectively using an oxidative treatment [4,7,12–14]. To determine the extent of catalyst deactivation other than by coke deposition, the used catalysts were regenerated by an oxidative regeneration in air at 680 °C for 12 h and subsequently characterized in detail. The characterization data (vide infra) reveal that dealumination of the H-ZSM-5 framework occurs, likely due to exposure with steam generated by dehydration of glycerol and oxygenated intermediates, in line with previous studies for H-ZSM-5(23) from our group [7,11].

Dealumination is particularly evident from solid-state NMR data for the regenerated H-ZSM-5 catalyst. Considerably higher values for the I_{EFAl}/I_{FAl} and $I_{Si(4Si,\ 0Al)}/I_{Si(3Si,\ 1Al)}$ were observed compared to the fresh H-ZSM-5 catalyst (Table S9). Besides, the intensity of the peak at δ = ca. 30 ppm (corresponding to the 5-coordinated EFAl) in the ^{27}Al MAS ssNMR spectrum of the regenerated H-ZSM-5 (Fig. 9-iii-c) is considerably higher than for fresh H-ZSM-5 (Fig. 9-iii-a). This indicates the occurrence of dealumination of H-ZSM-5 framework after reaction and regeneration, which leads to a lowering of the relative crystallinity (77%, Table 2) and a reduction in total acidity (670 μmol NH_3 g^{-1}H-ZSM-5, Table 2) for the regenerated H-ZSM-5 catalyst, though minor effects are detected regarding microporosity (Table S9) [7].

The three regenerated H-ZSM-5/binder catalysts also show considerably higher I_{EFAl}/I_{FAl} and $I_{Si(4Si,\ 0Al)}/I_{Si(3Si,\ 1Al)}$ values compared to the corresponding fresh ones (Fig. 7-i-iii-d and Table S9), indicating that dealumination of the H-ZSM-5 framework after the first cycle of reaction-regeneration cannot be eliminated by introducing a binder. In line with this statement is the observation of a reduced relative crystallinity (62–81%, Table 2) and total acidity (629–652 μmol NH_3 g^{-1} regenerated catalyst, Table 2) for the three regenerated H-ZSM-5/binder catalysts. Further studies will be required to assess the effect of irreversible deactivation of catalyst characteristics on catalyst performance by performing multiple reaction-regeneration cycles, which is beyond the scope of this investigation.

4. Conclusions

Shaped H-ZSM-5-based catalysts with various binders were prepared in a mini mixer/extruder (10 g $batch^{-1}$) and were applied for catalytic conversion of glycerol to bio-based aromatics (GTA) in a continuous tandem reactor, aiming to elucidate the effects of binders and shaping on catalyst performance. The use of such catalyst is of high relevance for scale-up and industrial implementation of MFI-type zeolite for the biomass conversion to biofuels and bio-based chemicals. It has so far not been reported for the conversion of glycerol to BTX, which makes this work novel and relevant.

The best results obtained here, though without optimization of the binder content, is over the H-ZSM-5/Al_2O_3 catalyst containing 10 wt% Al_2O_3. Catalyst life-time is enhanced considerably (at least 45%), though the peak BTX yield in the steady-state is slightly lower than for H-ZSM-5 alone. As such, the total BTX productivity (ca. 518 mg BTX g^{-1}H-ZSM-5) is considerably higher (70%) than for H-ZSM-5 alone (ca. 312 mg BTX g^{-1}H-ZSM-5), which is an important finding for future catalyst development and scale-up studies. Detailed catalyst characterization studies indicate that the prolonged life-time is likely due to a higher coke accommodation capacity of the mesoporous Al_2O_3 binder than microporous H-ZSM-5 (21 vs. 8 wt%), leading to a reduced coking rate of H-ZSM-5, which is the active catalyst for BTX formation.

Declaration of Competing Interest

The authors report no declarations of interest.

Acknowledgments

The Dutch Research Council (NWO) is acknowledged for the financial support (NWO-LIFT programme, Grant No. 731.016.401). Dr. K.S.S. Gupta (Leiden Institute of Chemistry, Leiden University), Dr. M.C.A. Stuart (Electron Microscopy Facility, University of Groningen), and J. van Dijken (Zernike Institute for Advanced Materials, University of Groningen) are thanked for their contributions in MAS ssNMR, HR-TEM-EDX, and TG-DTG analyses.

Appendix A. Supplementary data

Supplementary data to this article can be found online at https://doi.org/10.1016/j.fuproc.2021.106944.

References

[1] R. Ciriminna, C. Della Pina, M. Rossi, M. Pagliaro, Understanding the glycerol market, Eur. J. Lipid Sci. Technol. 116 (2014) 1432–1439, https://doi.org/10.1002/ejlt.201400229.
[2] C. Sivasankaran, P.K. Ramanujam, B. Balasubramanian, J. Mani, Recent progress on transforming crude glycerol into high value chemicals: a critical review, Biofuels-UK 10 (2016) 309–314, https://doi.org/10.1080/17597269.2016.1174018.
[3] X. Luo, X. Ge, S. Cui, Y. Li, Value-added processing of crude glycerol into chemicals and polymers, Bioresour. Technol. 215 (2016) 144–154, https://doi.org/10.1016/j.biortech.2016.03.042.
[4] S. He, I. Muizebelt, A. Heeres, N.J. Schenk, R. Blees, H.J. Heeres, Catalytic pyrolysis of crude glycerol over shaped ZSM-5/bentonite catalysts for bio-BTX synthesis, Appl. Catal. B 235 (2018) 45–55, https://doi.org/10.1016/j.apcatb.2018.04.047.
[5] C.M. Lok, J. Van Doorn, G.A. Almansa, Promoted ZSM-5 catalysts for the production of bio-aromatics, a review, Renew. Sust. Energ. Rev. 113 (2019) 1–11, https://doi.org/10.1016/j.rser.2019.109248. Article number 109248.
[6] T.Q. Hoang, X.L. Zhu, T. Danuthai, L.L. Lobban, D.E. Resasco, R.G. Mallinson, Conversion of glycerol to alkyl-aromatics over zeolites, Energy Fuel 24 (2010) 3804–3809, https://doi.org/10.1021/ef100160y.
[7] S. He, K. Zuur, D.S. Santosa, A. Heeres, C. Liu, E. Pidko, H.J. Heeres, Catalytic conversion of glycerol over an unmodified H-ZSM-5 zeolite to bio-based aromatics, Appl. Catal. B 281 (2021) 1–14, https://doi.org/10.1016/j.apcatb.2020.119467. Article number 119467.
[8] O. Muraza, Peculiarities of glycerol conversion to chemicals over zeolite-based catalysts, Front. Chem. 7 (2019) 1–11, https://doi.org/10.3389/fchem.2019.00233. Article number 233.
[9] F. Fantozzi, A. Frassoldati, P. Bartocci, G. Cinti, F. Quagliarini, G. Bidini, E. M. Ranzi, An experimental and kinetic modeling study of glycerol pyrolysis, Appl. Energy 184 (2016) 68–76, https://doi.org/10.1016/j.apenergy.2016.10.018.
[10] A.R. Maag, G.A. Tompsett, J. Tam, C.A. Ang, G. Azimi, A.D. Carl, X.L. Huang, L. J. Smith, R.L. Grimm, J.Q. Bond, M.T. Timko, ZSM-5 decrystallization and dealumination in hot liquid water, Phys. Chem. Chem. Phys. 21 (2019) 17880–17892, https://doi.org/10.1039/c9cp01490j.
[11] S. He, H.R. Goldhoorn, Z. Tegudeer, A. Chandel, A. Heeres, M.C.A. Stuart, H. J. Heeres, A time- and space-resolved catalyst deactivation study on the conversion of glycerol to aromatics using H-ZSM-5, submitted, 2021.
[12] A. Corma, G.W. Huber, L. Sauvanaud, P. O'Connor, Processing biomass-derived oxygenates in the oil refinery: Catalytic cracking (FCC) reaction pathways and role of catalyst, J. Catal. 247 (2007) 307–327, https://doi.org/10.1016/j.jcat.2007.01.023.
[13] N.N. Xu, D.H. Pan, Y.F. Wu, S.Q. Xu, L.J. Gao, J. Zhang, G.M. Xiao, Preparation of nano-sized HZSM-5 zeolite with sodium alginate for glycerol aromatization, React.

Kinet. Mech. Catal. 127 (2019) 449–467, https://doi.org/10.1007/s11144-019-01566-0.
[14] F. Wang, W.Y. Xiao, L.J. Gao, G.M. Xiao, Enhanced performance of glycerol to aromatics over Sn-containing HZSM-5 zeolites, RSC Adv. 6 (2016) 42984–42993, https://doi.org/10.1039/c6ra03358j.
[15] F. Wang, M.-x. Zhou, X.-h. Yang, L.-j. Gao, G.-m. Xiao, The effect of hierarchical pore architecture on one-step catalytic aromatization of glycerol: Reaction routes and catalytic performances, Mol. Catal. 432 (2017) 144–154, https://doi.org/10.1016/j.mcat.2017.01.017.
[16] F. Wang, X.Z. Chu, P.S. Zhao, F.X. Zhu, Q.Q. Li, F.Y. Wu, G.M. Xiao, Shape selectivity conversion of biomass derived glycerol to aromatics over hierarchical HZSM-5 zeolites prepared by successive steaming and alkaline leaching: Impact of acid properties and pore constraint, Fuel 262 (2020) 1–9, https://doi.org/10.1016/j.fuel.2019.116538. Article number 116538.
[17] D.H. Pan, S.Q. Xu, Y.A. Miao, N.N. Xu, H.Z. Wang, X.H. Song, L.J. Gao, G.M. Xiao, A highly active and stable Zn@C/HZSM-5 catalyst using Zn@C derived from ZIF-8 as a template for conversion of glycerol to aromatics, Catal. Sci. Technol. 9 (2019) 739–752, https://doi.org/10.1039/c8cy02217h.
[18] A. Errekatxo, A. Ibarra, A. Gutierrez, J. Bilbao, J.M. Arandes, P. Castano, Catalytic deactivation pathways during the cracking of glycerol and glycerol/VGO blends under FCC unit conditions, Chem. Eng. J. 307 (2017) 955–965, https://doi.org/10.1016/j.cej.2016.08.100.
[19] S. Mitchell, N.L. Michels, J. Perez-Ramirez, From powder to technical body: the undervalued science of catalyst scale up, Chem. Soc. Rev. 42 (2013) 6094–6112, https://doi.org/10.1039/c3cs60076a.
[20] V.R. Choudhary, C. Sivadinarayana, K. Mantri, Influence of catalyst binder on the acidity and activity/selectivity of Ga/H-ZSM-5 zeolite in propane aromatization, Proc. Indian Acad. Sci. Chem. Sci. 111 (1999) 669–676, https://doi.org/10.1007/BF02869122.
[21] M. Falco, E. Morgado, N. Amadeo, U. Sedran, Accessibility in alumina matrices of FCC catalysts, Appl. Catal. A 315 (2006) 29–34, https://doi.org/10.1016/j.apcata.2006.08.028.
[22] J.S.J. Hargreaves, A.L. Munnoch, A survey of the influence of binders in zeolite catalysis, Catal. Sci. Technol. 3 (2013) 1165–1171, https://doi.org/10.1039/c3cy20866d.
[23] C. Chen, H. Ji, Q. Zhang, C. Li, H. Shan, Effect of gamma-alumina as active matrix added to HZSM-5 catalyst on the aromatization of methanol, Appl. Petrochem. Res. 5 (2015) 231–243, https://doi.org/10.1007/s13203-015-0139-5.
[24] H. Hernando, C. Ochoa-Hernandez, M. Shamzhy, I. Moreno, J. Fermoso, P. Pizarro, J.M. Coronado, J. Cejka, D.P. Serrano, The crucial role of clay binders in the performance of ZSM-5 based materials for biomass catalytic pyrolysis, Catal. Sci. Technol. 9 (2019) 789–802, https://doi.org/10.1039/c8cy02116c.
[25] S.P. Verkleij, G.T. Whiting, D. Pieper, S.P. Esclapez, S.W. Li, M.M. Mertens, M. Janssen, A.J. Bons, M. Burgers, B.M. Weckhuysen, Chemical imaging of the binder-dependent coke formation in zeolite-based catalyst bodies during the transalkylation of aromatics, Chemcatchem 11 (2019) 4788–4796, https://doi.org/10.1002/cctc.201900777.
[26] N.L. Michels, S. Mitchell, J. Perez-Ramirez, Effects of binders on the performance of shaped hierarchical MFI zeolites in methanol-to-hydrocarbons, ACS Catal. 4 (2014) 2409–2417, https://doi.org/10.1021/cs500353b.
[27] G.T. Whiting, A.D. Chowdhury, R. Oord, P. Paalanen, B.M. Weckhuysen, The curious case of zeolite-clay/binder interactions and their consequences for catalyst preparation, Faraday Discuss. 188 (2016) 369–386, https://doi.org/10.1039/c5fd00200a.
[28] G.T. Whiting, F. Meirer, M.M. Mertens, A.J. Bons, B.M. Weiss, P.A. Stevens, E. de Smit, B.M. Weckhuysen, Binder effects in SiO_2- and Al_2O_3-bound zeolite ZSM-5-based extrudates as studied by microspectroscopy, Chemcatchem 7 (2015) 1312–1321, https://doi.org/10.1002/cctc.201402897.
[29] L.H. Dao, M. Haniff, A. Houle, D. Lamothe, Reactions of model compounds of biomass-pyrolysis oils over ZSM-5 zeolite catalysts, ACS Symp. Ser. 376 (1988) 328–341.
[30] J.J. Zhao, J. Zhou, Y. Chen, Q.J. He, M.L. Ruan, L.M. Guo, J.L. Shi, H.R. Chen, Fabrication of mesoporous zeolite microspheres by a one-pot dual-functional templating approach, J. Mater. Chem. 19 (2009) 7614–7616, https://doi.org/10.1039/b916862a.
[31] O. Solcova, L. Matejova, P. Topka, Z. Musilova, P. Schneider, Comparison of textural information from argon (87 K) and nitrogen (77 K) physisorption, J. Porous. Mater. 18 (2011) 557–565, https://doi.org/10.1007/s10934-010-9409-x.
[32] K.S.W. Sing, D.H. Everett, R.A.W. Haul, L. Moscou, R.A. Pierotti, J. Rouquerol, T. Siemieniewska, Reporting physisorption data for gas/solid systems with special reference to the determination of surface area and porosity, Pure Appl. Chem. 57 (1985) 603–619, https://doi.org/10.1351/pac198254112201.
[33] D. Li, Y. Chen, J. Hu, B. Deng, X. Cheng, Y. Zhang, Synthesis of hierarchical chabazite zeolite via interzeolite transformation of coke-containing spent MFI, Appl. Catal. B 270 (2020) 1–11, https://doi.org/10.1016/j.apcatb.2020.118881. Article number 118881.
[34] L.P. Wu, X.J. Li, Z.H. Yuan, Y. Chen, Fabrication and characterization of titanate nanotube supported ZSM-5 zeolite composite catalyst for ethanol dehydration to ethylene, Bull. Kor. Chem. Soc. 35 (2014) 525–530, https://doi.org/10.5012/bkcs.2014.35.2.525.
[35] P.F. Corregidor, D.E. Acosta, H.A. Destefanis, Green synthesis of ZSM-5 zeolite prepared by hydrothermal treatment of perlite. Effect of chemical composition and characterization of the product, Sci. Adv. Mater. 6 (2014) 1203–1214, https://doi.org/10.1166/sam.2014.1894.
[36] J.C. Groen, L.A.A. Peffer, J. Perez-Ramirez, Pore size determination in modified micro- and mesoporous materials. Pitfalls and limitations in gas adsorption data analysis, Microporous Mesoporous Mater. 60 (2003) 1–17, https://doi.org/10.1016/s1387-1811(03)00339-1.
[37] J.P.H. Li, A.A. Adesina, E.M. Kennedy, M. Stockenhuber, A mechanistic study of the Knoevenagel condensation reaction: new insights into the influence of acid and base properties of mixed metal oxide catalysts on the catalytic activity, Phys. Chem. Chem. Phys. 19 (2017) 26630–26644, https://doi.org/10.1039/c7cp04743f.
[38] W.Y. Li, H. Qian, R. Liu, X.L. Zhao, Z. Tang, X.H. Huang, W.H. Li, X.M. Chen, F. Z. Xie, W.S. Zou, Q.S. Qu, Controlled manipulation of TiO_2 nanoclusters inside mesochannels of core-shell silica particles as stationary phase for HPLC separation, Microchim. Acta 187 (2020) 1–9, https://doi.org/10.1007/s00604-020-04268-w. Article number 328.
[39] Q. Bkour, N. Faqir, R. Shawabkeh, A. Ul-Hamid, H.J. Bart, Synthesis of a Ca/Na-aluminosilicate from kaolin and limestone and its use for adsorption of CO2, J. Environ. Chem. Eng. 4 (2016) 973–983, https://doi.org/10.1016/j.jece.2015.12.039.
[40] A.S. Al-Dughaither, H. de Lasa, HZSM-5 zeolites with different SiO_2/Al_2O_3 ratios. Characterization and NH_3 desorption kinetics, Ind. Eng. Chem. Res. 53 (2014) 15303–15316, https://doi.org/10.1021/ie4039532.
[41] A. Guatame-Garcia, M. Buxton, F. Deon, C. Lievens, C. Hecker, Toward an on-line characterization of kaolin calcination process using short-wave infrared spectroscopy, Miner. Process. Extr. Metall. Rev. 39 (2018) 420–431, https://doi.org/10.1080/08827508.2018.1459617.
[42] S. He, F.G.H. Klein, T.S. Kramer, A. Chandel, Z. Tegudeer, A. Heeres, H.J. Heeres, Catalytic conversion of free fatty acids to bio-based aromatics: a model investigation using oleic acid and an H-ZSM-5/Al_2O_3 catalyst, ACS Sustain. Chem. Eng. 9 (2021) 1128–1141, https://doi.org/10.1021/acssuschemeng.0c06181.
[43] M.I. Zaki, M.A. Hasan, F.A. Al-Sagheer, L. Pasupulety, In situ FTIR spectra of pyridine adsorbed on SiO_2-Al_2O_3, TiO_2, ZrO_2 and CeO_2: general considerations for the identification of acid sites on surfaces of finely divided metal oxides, Colloids Surf. A Physicochem. Eng. Asp. 190 (2001) 261–274, https://doi.org/10.1016/s0927-7757(01)00690-2.
[44] K. Ramesh, C. Jie, Y.F. Han, A. Borgna, Synthesis, characterization, and catalytic activity of phosphorus modified H-ZSM-5 catalysts in selective ethanol dehydration, Ind. Eng. Chem. Res. 49 (2010) 4080–4090, https://doi.org/10.1021/ie901666f.
[45] Z.W. Yu, S.H. Li, Q. Wang, A.M. Zheng, X. Jun, L. Chen, F. Deng, Bronsted/Lewis acid synergy in H-ZSM-5 and H-MOR zeolites studied by H-1 and Al-27 DQ-MAS solid-state NMR spectroscopy, J. Phys. Chem. C 115 (2011) 22320–22327, https://doi.org/10.1021/jp203923z.
[46] V.R. Choudhary, P. Devadas, A.K. Kinage, M. Guisnet, Influence of binder on the acidity and performance of H-Gallosilicate (MFI) zeolite in propane aromatization, Appl. Catal. A 162 (1997) 223–233, https://doi.org/10.1016/S0926-860X(97)00100-2.
[47] J. Zhou, J. Teng, L. Ren, Y. Wang, Z. Liu, W. Liu, W. Yang, Z. Xie, Full-crystalline hierarchical monolithic ZSM-5 zeolites as superiorly active and long-lived practical catalysts in methanol-to-hydrocarbons reaction, J. Catal. 340 (2016) 166–176, https://doi.org/10.1016/j.jcat.2016.05.009.
[48] S.M. Danov, A.L. Esipovich, A.S. Belousov, A.E. Rogozhin, Deactivation of acid catalysts in vapor-phase dehydration of glycerol into acrolein, Russ. J. Appl. Chem. 87 (2014) 461–467, https://doi.org/10.1134/s10704272140400119.
[49] F. Bauer, H.G. Karge, Characterization of coke on zeolites, in: H.G. Karge, J. Weitkamp (Eds.), Molecular Sieves Volume 5: Characterization II, Springer-Verlag, Berlin Heidelberg, Heidelberg, 2007, pp. 249–364, https://doi.org/10.1007/3829_005.